

See discussions, stats, and author profiles for this publication at: <https://www.researchgate.net/publication/262538985>

Structure of a Dihydroxycoumarin Active-Site Inhibitor in Complex with the RNase H Domain of HIV-1 Reverse Transcriptase and Structure-Activity Analysis of Inhibitor Analogs

ARTICLE *in* JOURNAL OF MOLECULAR BIOLOGY · MAY 2014

Impact Factor: 4.33 · DOI: 10.1016/j.jmb.2014.05.006 · Source: PubMed

CITATIONS

2

READS

28

7 AUTHORS, INCLUDING:



[Daniel M Himmel](#)

Albert Einstein College of Medicine

23 PUBLICATIONS 1,312 CITATIONS

[SEE PROFILE](#)



[Tatiana Ilina](#)

University of Pittsburgh

10 PUBLICATIONS 173 CITATIONS

[SEE PROFILE](#)



[Alexander Van Ry](#)

1 PUBLICATION 2 CITATIONS

[SEE PROFILE](#)

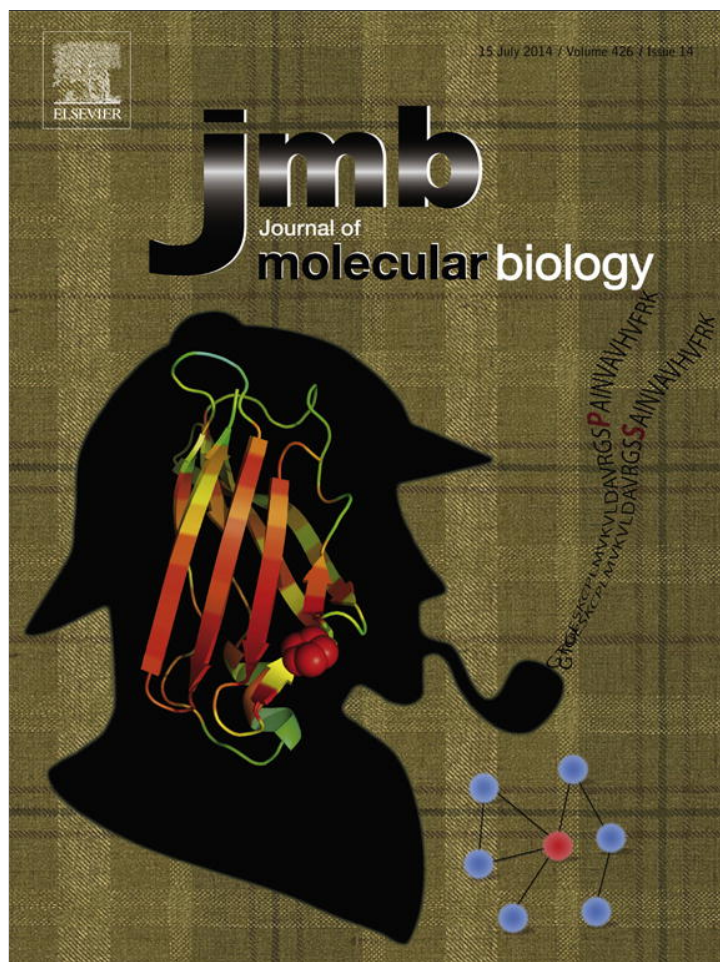


[Eddy Arnold](#)

Rutgers, The State University of New Jersey

255 PUBLICATIONS 15,130 CITATIONS

[SEE PROFILE](#)

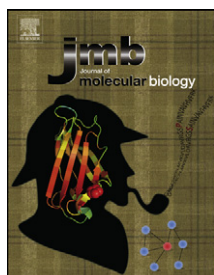


This article appeared in a journal published by Elsevier. The attached copy is furnished to the author for internal non-commercial research and education use, including for instruction at the authors institution and sharing with colleagues.

Other uses, including reproduction and distribution, or selling or licensing copies, or posting to personal, institutional or third party websites are prohibited.

In most cases authors are permitted to post their version of the article (e.g. in Word or Tex form) to their personal website or institutional repository. Authors requiring further information regarding Elsevier's archiving and manuscript policies are encouraged to visit:

<http://www.elsevier.com/authorsrights>



Structure of a Dihydroxycoumarin Active-Site Inhibitor in Complex with the RNase H Domain of HIV-1 Reverse Transcriptase and Structure–Activity Analysis of Inhibitor Analogs

Daniel M. Himmel¹, Nataliya S. Myshakina², Tatiana Ilina², Alexander Van Ry², William C. Ho¹, Michael A. Parniak² and Eddy Arnold¹

1 - Center for Advanced Biotechnology and Medicine and Department of Chemistry and Chemical Biology, Rutgers University, Piscataway, NJ 08854-5627, USA

2 - Department of Microbiology and Molecular Genetics, University of Pittsburgh School of Medicine, Pittsburgh, PA 15219, USA

Correspondence to Eddy Arnold: Center for Advanced Biotechnology and Medicine and Department of Chemistry and Chemical Biology, Rutgers University, 679 Hoes Lane West, Piscataway, NJ 08854-5627, USA. arnold@cabm.rutgers.edu
<http://dx.doi.org/10.1016/j.jmb.2014.05.006>

Edited by E. O. Freed

Abstract

Human immunodeficiency virus (HIV) encodes four essential enzymes: protease, integrase, reverse transcriptase (RT)-associated DNA polymerase, and RT-associated ribonuclease H (RNase H). Current clinically approved anti-AIDS drugs target all HIV enzymatic activities except RNase H, which has proven to be a very difficult target for HIV drug discovery. Our high-throughput screening activities identified the dihydroxycoumarin compound F3284-8495 as a specific inhibitor of RT RNase H, with low micromolar potency *in vitro*. Optimization of inhibitory potency can be facilitated by structural information about inhibitor–target binding. Here, we report the crystal structure of F3284-8495 bound to the active site of an isolated RNase H domain of HIV-1 RT at a resolution limit of 1.71 Å. From predictions based on this structure, compounds were obtained that showed improved inhibitory activity. Computational analysis suggested structural alterations that could provide additional interactions with RT and thus improve inhibitory potency. These studies established proof of concept that F3284-8495 could be used as a favorable chemical scaffold for development of HIV RNase H inhibitors.

© 2014 Elsevier Ltd. All rights reserved.

Introduction

Drugs that target human immunodeficiency virus (HIV) reverse transcriptase (RT) are critical components of highly active antiretroviral therapy (known as HAART) used to treat HIV infection [1,2]. HIV RT converts the single-stranded viral genomic RNA to the double-stranded viral DNA form that is then integrated into the infected host cell genome, an essential process in the HIV replication cycle. The conversion of HIV genomic RNA to DNA is a complex process entirely catalyzed by RT. RT RNA-dependent DNA polymerase (RDDP) activity synthesizes a complementary DNA copy of the HIV RNA template, ribonuclease H (RNase H) activity degrades the RNA strand in the DNA:RNA heteroduplex formed by the RT RDDP activity, and RT DNA-dependent DNA polymerase

activity converts the newly synthesized single-stranded DNA into double-stranded viral DNA. This process requires RT to be multifunctional, with both DNA polymerase and RNase H activities. In HIV RT, the active sites for these two different activities are located in different protein domains and are separated by over 50 Å (Fig. 1). Both activities are essential for HIV replication [4,5]; yet, all current RT-directed therapeutics target only RT DNA polymerase activity. The continued emergence of HIV variants resistant to these and all other clinically used drugs [6–10] underscores the need to develop drugs against new targets such as RNase H that may be effective against resistant viruses. Despite considerable effort, no clinically useful drugs targeting RT RNase H have been developed.

RT RNase H has proven to be a difficult target for drug discovery and development. Structural

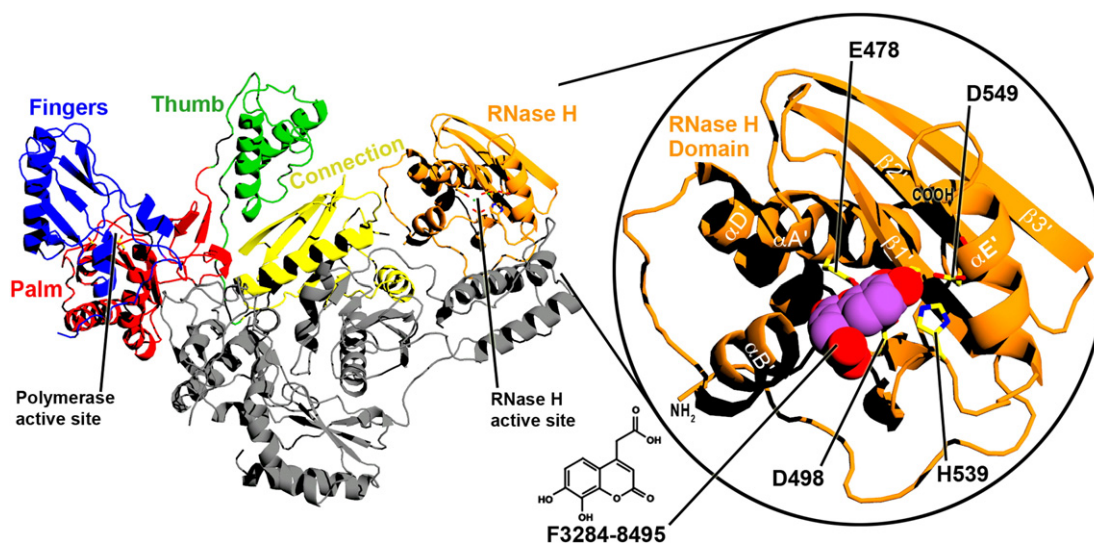


Fig. 1. Ribbon diagram of the structure of full-length RT. RT is a heterodimer that consists of p66 (color) and p51 (gray) subunits. The two enzymatic active sites and the subdomains of the p66 subunit are labeled. Right inset: A closer view of the isolated RNase H domain of the current structure, with F3284-8495 bound at the active site. Selected α -helices and β -sheets are labeled based on Ref. [3]. The chemical structure of F3284-8495 is shown at the bottom center of the figure.

information about the interaction of RNase H inhibitors (RNHIs) identified in screening activities with RT may facilitate the development and optimization of RNHIs with potential clinical utility. X-ray crystal structures have been reported for a number of RNHIs in complex with full-length RT and/or the isolated HIV-1 RNase H domain, including one allosteric inhibitor [11] and several RNase H active-site inhibitors [12–17]. However, none of these RNase H active-site-directed inhibitors show substantial antiviral activity, and the search continues for chemical scaffolds that readily facilitate synthesis of compounds that can be tested for inhibitory activity. Compound F3284-8495 [IUPAC name: (7,8-dihydroxy-2-oxo-2H-chromen-4-yl)acetic acid] is a dihydroxycoumarin that exhibits low micromolar inhibition of the RNase H activity of RT without significant inhibition of RT polymerase activity. We here report an X-ray crystal structure at a 1.71-Å-resolution limit for F3284-8495 in complex with the isolated RNase H domain of HIV-1 RT (Figs. 1 and 2). The inhibitor has a chemically modifiable ethanoic acid substituent positioned in the crystal complex in such a manner as to present opportunities for structural analogs that can form additional protein contacts. Several such analogs were obtained and evaluated for inhibitory potency *in vitro*. We also present a computational docking analysis of some of these analogs, based on the crystal structure, to deduce the binding mode that most likely accounts for their improved inhibitory activities and to suggest strategies for developing inhibitors based on the dihydroxycoumarin scaffold.

Results

F3284-8495 binds at the RNase H active site

The RNase H domain crystallized in the space group $P3_1$, with two RNase H molecules per asymmetric unit (Table 1). Several highly conserved residues in the RNase H active site are required for catalysis, including four carboxylic acids (Asp443, Glu478, Asp498, and Asp549) and His539 [4,22,23]. The four residues with carboxylate side chains have been shown to coordinate one or two divalent cations [12–17,24,25]. Our data provide unambiguous difference Fourier ($F_o - F_c$) electron density for F3284-8495 at the RNase H active site, along with strong electron density peaks for two Mn^{2+} cations separated by a distance of about 3.7 Å (Figs. 2 and 3). The cations are coordinated both by the inhibitor and by the four active-site carboxylates (Asp443, Glu478, Asp498, and Asp549). According to the two-cation mechanism hypothesis, the Mn^{2+} cations are conventionally designated as cations “A” and “B” [26,27]. Both divalent cations have approximately octahedral coordination geometry, including six to seven oxygen atoms from the inhibitor, active-site side chains, and two water molecules (Fig. 3). For cation A, one octahedral axis is formed by the two water molecules. The four other coordinating oxygen atoms comprise the two coumarin ring hydroxyls and a carboxyl oxygen atom from each of Asp549 and Asp443, with a coordinating distance ranging from 2.0 to 2.2 Å. The remaining Asp443 side-chain oxygen and the

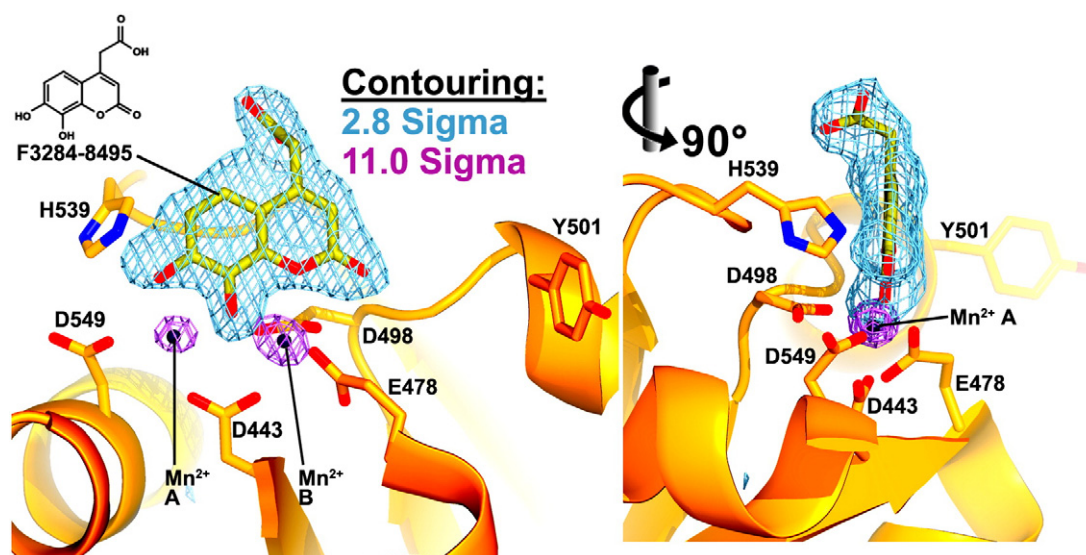


Fig. 2. Inhibitor electron density at the RNase H active site. Two $F_o - F_c$ simulated annealing omit maps are shown at the RNase H active site. In one (light blue, contoured at 2.8σ), the inhibitor has been excluded from the phase calculation, and in the other (violet, contoured at 11σ), both the Mn^{2+} cations and the inhibitor have been omitted from phasing. F3284-8495 (yellow carbon atoms) and two Mn^{2+} cations (black orbs) are shown modeled into the electron density. The cations are designated A and B. Two vantage points are shown rotated 90° from each other about the vertical axis.

coumarin ether oxygen of F3284-8495 form an octahedral axis for cation B. The four other coordinating atoms for cation B are one coumarin hydroxyl, both side-chain carboxyl oxygens of Asp498, and at least one side-chain carboxyl oxygen of Asp478. The coordinating distances for cation B range from 2.0 to 2.6 Å. The octahedral coordination sphere about cation B is non-ideal. A second Asp478 side-chain carboxyl oxygen forms a longer distance contact with cation B of 3.2–3.3 Å (Fig. 3). The cation coordination geometry observed in this structure agrees well with

the coordination geometry observed in several structures of HIV RNase H ligand complexes reported by Lansdon *et al.* [17] at resolutions ranging from 1.4 Å to 2.1 Å, including the positions of the Mn^{2+} cations and contact distances. In the Lansdon *et al.* structures, however, only one of the side-chain carboxyl oxygens of Asp498 coordinates cation B. As a result, Lansdon *et al.* count only five coordinating oxygen atoms about cation B, whereas we count six coordinating oxygen atoms. In addition to coordinating the cations, residues Glu478, Asp498, Asp549, and His539 form

Table 1. Crystallographic data collection and refinement statistics

Unit cell dimensions and space group	$a = 51.2 \text{ \AA}$, $b = 51.2 \text{ \AA}$, $c = 112.1 \text{ \AA}$	$\alpha = 90.0^\circ$, $\beta = 90.0^\circ$, $\gamma = 120^\circ$	$P3_1$
PDB ID code: 4QAG		Refinement	
Data collection		Resolution range used (Å)	28.6–1.71
Resolution limit (Å)	40–1.71	Completeness in range (%)	98.3
Unique reflections	34,856	Sigma cutoff	0.0
Completeness (%) / multiplicity		R -factor/ R_{free} (%)	18.2/19.0
All data	98.5/7.8	Cross-validated coordinate	
2.03- to 2.15-Å Shell	99.7/7.2	Error (Å) [18–20]	0.23
1.93- to 1.84-Å Shell	99.3/5.3	No. of protein/solvent atoms	2076/174
1.84- to 1.77-Å Shell	97.6/4.2	No. of inhibitor/cation atoms	34/4
1.77- to 1.71-Å Shell	89.5/2.9	RMS bond lengths (Å) [21]	0.008
R_{sym} (%) / average I/σ		RMS bond angles (°) [21]	0.94
All data	8.8/27.1	Average B -factors (Å ²)	
2.03- to 2.15-Å Shell	16.3/9.3	Protein/solvent	55.5/70.3
1.93- to 1.84-Å Shell	31.0/4.8	Inhibitor/cations	61.5/46.0
1.84- to 1.77-Å Shell	42.5/3.1	Ramachandran regions (%)	
1.77- to 1.71-Å Shell	45.1/2.4	Most favored	98.1
		Additional Allowed	1.9
		Generous or disallowed	0

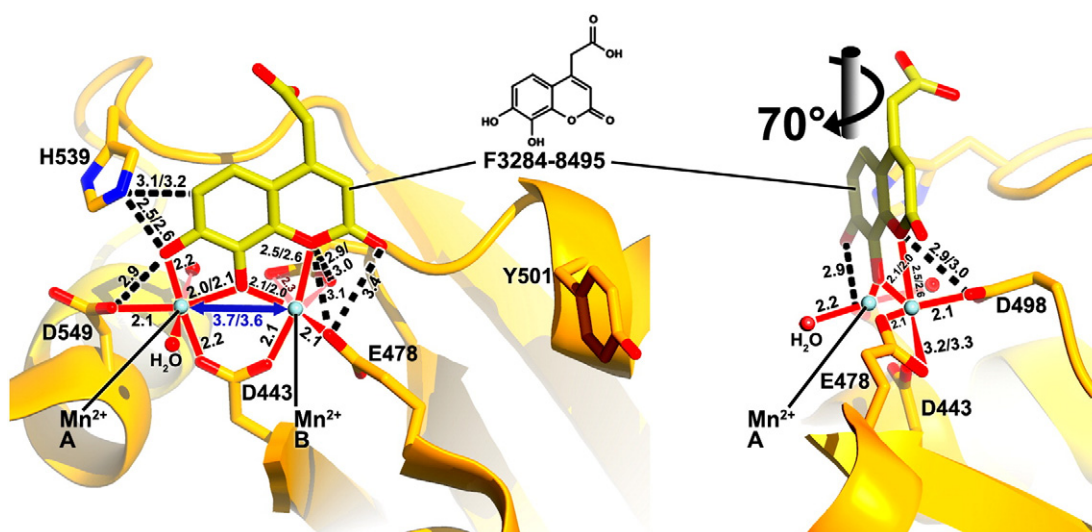


Fig. 3. Interactions between the protein, cations, and inhibitor. Coordination about the cations (light blue orbs) is shown as red continuous lines. Two water molecules participate in this coordination (red orbs). The separation distance between the cations is shown in blue. Black dashes designate protein–inhibitor contacts. Distances are in angstroms. Wherever the distances differ for each of the two protein–inhibitor complexes in the asymmetric unit, both distances are given. Two vantage points are given, rotated about 70° about the vertical axis.

hydrophobic or hydrogen-bonding contacts directly with the inhibitor. In some previous structures for RNHIs in complex with the isolated RNase H domain, the side chain of Arg557 formed a salt bridge with Asp549 [14,17]. This interaction is not seen, however, in the F3284-8495/RNase H domain complex. Compared to RT structures without an inhibitor bound at

the RNase H active site, the current structure shows no overall change in the conformation of the RNase H domain (Fig. 4a). The conformation of the RNase H active site is similar with and without bound ligand except that the side chain of Glu478 points away from the active site if divalent cation B is not present (Fig. 4b).

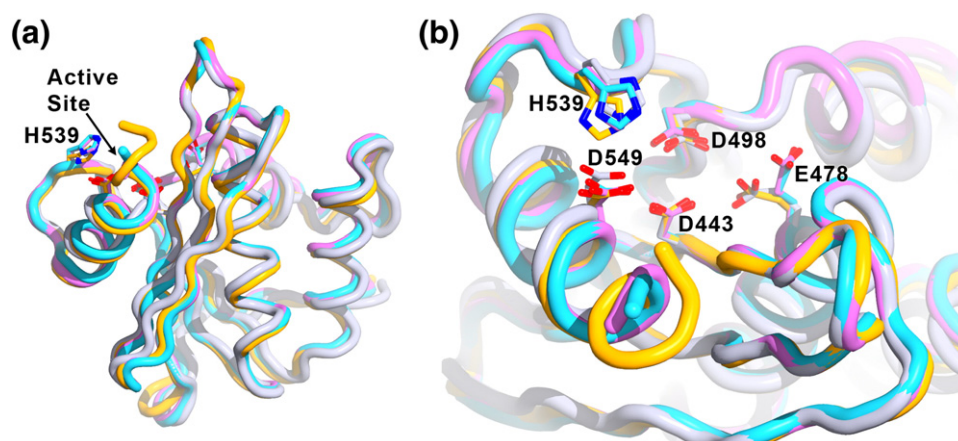


Fig. 4. Effect of F3284-8495 and cations on RNase H conformation. Shown is the superposition of the current structure (orange, inhibitor not shown) with the RNase H domain of several RT structures without inhibitors bound at the RNase H active site (referenced here by Protein Data Bank accession numbers): 3DLK [28] (cyan), with no ligands bound; 4G1Q [29] (violet), with Mg^{2+} bound at the cation A position; and 2BE2 [30] (gray), with Mn^{2+} bound at the cation B position. Superposition is based on main-chain atoms for residues 441–448 of the RNase H domain. (a) A view of the entire RNase H domain. The overall conformation of the RNase H domain is highly similar whether or not ligands are bound. (b) A closer view of the active site, rotated toward the viewer by about 60°. Glu478 tends to point away from the active site if there is no cation B to coordinate (3DLK and 4G1Q). His539 may adjust its position and side-chain conformation to interact with a ligand such as F3284-8495 at the active site.

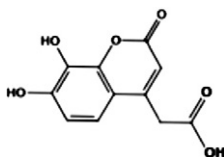
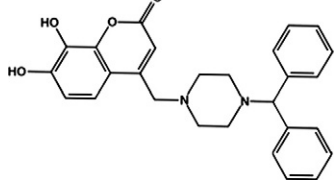
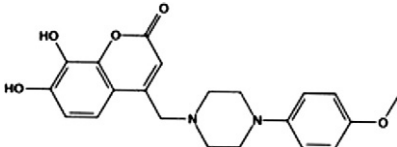
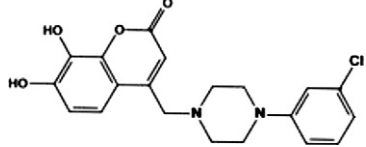
Binding and inhibitory properties

F3284-8495 inhibited the RNase H activity of the p66/p51 RT heterodimer *in vitro* with an IC_{50} of 4.8 μ M when assayed under putative physiological conditions (pH 7.4, 1 mM Mg^{2+}) (Table 2). The compound showed higher inhibitory activity (IC_{50} = 1.1 μ M) when assayed under conditions optimal for RNase H activity (pH 8.0, 10 mM Mg^{2+}). F3284-8495 exhibited no detectable inhibition of RT DNA polymerase activity at 10 μ M, the highest concentration tested. Surprisingly, this compound was a poor inhibitor of a catalytically active HIV RNase H domain fragment (IC_{50} > 10 μ M). This enzyme construct, termed p15-EC, was created by replacing a small loop segment of HIV-1 RT RNase H with a 24-residue α -helical substrate-binding loop derived from *Escherichia coli* RNase HI and has been widely used to screen RNHIs and characterize protein–inhibitor interactions [31–34].

Based on the structure reported here, we obtained a series of analogs of F3284-8495 in which the ethanoic acid substituent was replaced with a variety of bulkier substituents anticipating that these might

form additional contacts with the RNase H protein and thus improve inhibitory potency. Most of the analogs showed similar or only slightly increased potency for inhibition of RT-associated RNase H activity compared to F3284-8495 (Table S1). However, the most potent of the analogs, F3385-2590, inhibited RT RNase H activity under physiological assay conditions with an *in vitro* IC_{50} of about 0.8 μ M, a 6-fold increase in inhibitory potency compared to the parent compound. This compound also inhibited the DNA polymerase activity of RT to a lesser extent. Compound F3385-2588 inhibited RT RNase H activity with an *in vitro* IC_{50} of 2.1 μ M at pH 7.4 and 0.7 μ M at pH 8 but did not inhibit the DNA polymerase activity of RT. Unlike the parent compound F3284-8495, most of the analogs inhibited the catalytically active p15-EC RT RNase H domain fragment (Table S1). Two of the compounds, F3385-2581 and F3385-2590, showed nanomolar inhibitory potency against p15-EC RNase H (Table 2). The increased inhibitory activity of these analogs against the RNase H domain fragment is consistent with the structural predictions arising from the RNase H/F3284-8495 crystal structure reported

Table 2. *In vitro* inhibitory properties of F3284-8495 and selected analogs

Compound	Structure	<i>In vitro</i> IC_{50} (μ M) ^a			
		RT RNase H		p15-EC RNase H ^b	RT DNA pol ^b
		pH 7.4, 1 mM Mg^{2+}	pH 8.0, 10 mM Mg^{2+}		
F3284-8495		4.8	1.1	>10	>10
F3385-2581		2.2	1.9	0.1	2.2
F3385-2588		2.1	0.7	1.5	>10
F3385-2590		0.8	0.4	0.2	2.5

^a Data are the averages of two separate determinations, each carried out over a series of at least eight different concentrations.

^b Assayed at pH 7.4, 1 mM Mg^{2+} .

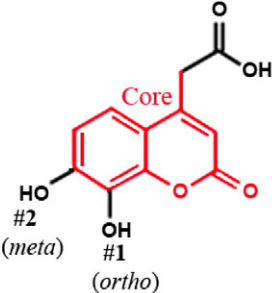
in the present work because the analogs can form contacts with additional residues in the RT RNase H domain.

Docking experiments

To better understand the binding of F3284-8495 and the improved activity of some of its derivatives, we conducted computational docking experiments using the Glide module of the Schrödinger Software suite. Since the two hydroxyls on the coumarin ring system of F3284-8495 are acidic, all possible coumarin ring protonation states of the inhibitor were generated for completeness and docked to the

active site. The resulting Glide docking scores were compared, and the docked models were superimposed on the crystal structure for comparison (Table 3). Deprotonation of the *ortho* hydroxyl alone led to good docking scores and the best agreement with the crystal structure, with a coumarin core root-mean-square (RMS) deviation ranging from 0.17 to 0.26 Å, and excellent superposition on visual inspection. The best docking scores were obtained with deprotonation of both hydroxyls, but the predicted binding positions did not agree as well with the crystal structure, giving an RMS deviation of 0.21–0.31 and good (but not excellent) superposition on visual inspection. By contrast, *protonation* of either the

Table 3. Protonation effect on the docking of F3284-8495 to the RNase H active site

<p>Notation:</p> <p>p_{rt} = protonated d_{p_{rt}} = deprotonated</p> <div>  </div>			
Protonation state	Best docking scores	Core RMS difference from crystal structure ^a	Quality of core superposition by visual inspection
1d _{p_{rt}} -2d _{p_{rt}}	-8.69 -8.64 -8.63 -8.57	0.309 0.249 0.268 0.212	Good superposition " " Very good superposition
2p _{rt} -1d _{p_{rt}}	-8.18 -8.09 -8.08 -8.07	0.260 0.184 0.189 0.172	Very good superposition Excellent superposition " "
1p _{rt} -2d _{p_{rt}}	-6.77 -6.09 -6.08 -5.83	0.414 0.330 0.338 0.294	Fair superposition " " "
1p _{rt} -2p _{rt}	-3.43 -3.35 -3.32 -3.25	0.927 0.919 0.458 0.908	Poor superposition " Fair superposition Poor superposition

^a Superposition for RMS calculations was based on the main-chain atoms for residues 441–444.

ortho hydroxyl alone or both hydroxyls led to poor predictions of binding. Thus, it appears that the *ortho* hydroxyl of the inhibitor is likely to be deprotonated in order to approximate the binding mode observed in the crystal structure. Deprotonation of the second (*meta*) hydroxyl may occur less frequently at physiological pH.

The ethanoic acid group of F3284-8495 is attached to the coumarin ring system by a freely rotatable single bond. As a result, for a number of F3284-8495 derivatives reported here, the substructures that replace the ethanoic acid substituent of F3284-8495 are long enough (8–10 Å) to bring them within reach of additional residue contacts near the RNase H active site. These include Gln500 (which has recently been proposed as a possible binding site for allosteric RNHIs [35]), Trp535, Arg448, and, importantly, active-site residue His539. The most potent derivatives F3385-2581, F3385-2588, and F3385-2590 (Table 2) were selected for induced-fit docking analysis. In all of these structures, the ethanoic acid substituent of F3284-8495 is replaced by a piperazine ring linked to one or more aromatic rings. The conformers with the top Glide scores and coumarin cores that superimposed well on that of the crystal structure are shown in Figs. 5–7.

The piperazine ring of F3385-2581 is linked via a branch point to two phenyl rings. For this compound, a single high-scoring docking conformation (pose) was obtained (Fig. 5). In that pose, the two phenyl rings formed hydrophobic side-chain interactions with Trp535, Ala538, and Lys540; main-chain and side-chain interactions with Pro537, as well as side-chain contacts with p51 subunit residue Leu422. Electrostatic interactions with the side chain of Gln500, the main

chain of Ala538, and the side chain of p51 subunit residue Asn265 were also noted. The total free energy contributions from the electrostatic interactions were predicted to be energetically slightly more favorable (by about 5 kcal/mol) than the combined free energy contributions of the hydrophobic contacts. An induced-fit Glide docking score of –10.25 kcal/mol was obtained for this binding mode.

Both compounds F3385-2588 and F3385-2590 gave better docking scores for their top-ranked results. In compound F3385-2588 (Fig. 6), the piperazine ring is linked to a *para*-methoxyphenyl ring. Compound F3385-2590 is similar, except that the *para*-methoxyphenyl ring is replaced with a *meta*-chlorophenyl ring (Fig. 7). Both of these compounds gave similar docking results. In the best-scoring pose (Figs. 6 and 7, pose group 1), the combined free energy contribution from hydrophobic contacts was equal or greater than that of the electrostatic interactions. The docked structures predicted interactions of the piperazine-phenyl ring system with RNase H residues Trp535, Pro537, and Ala538, as well as residue Asn265 of the p51 subunit of RT. F3385-2588 (pose group 1) also interacted Lys540 and with p51 residue Gly262 (Fig. 6). The docking study also predicted alternative ligand conformations (Figs. 6 and 7, pose groups 2 and 3) that could interact with residues such as Gln475 or Tyr501 and residues that help position the scissile phosphate of the substrate RNA strand at the RNase H active site, such as Arg448 or Asn474 [36]. Gln475 and Tyr501 are part of the so-called “RNase H primer grip”, which in RT also includes p66 residues Gly359, Ala360, His361, Thr473, Lys476, and Ile505, as well as p51 residues Lys395 and Glu396. The RNase H primer grip residues

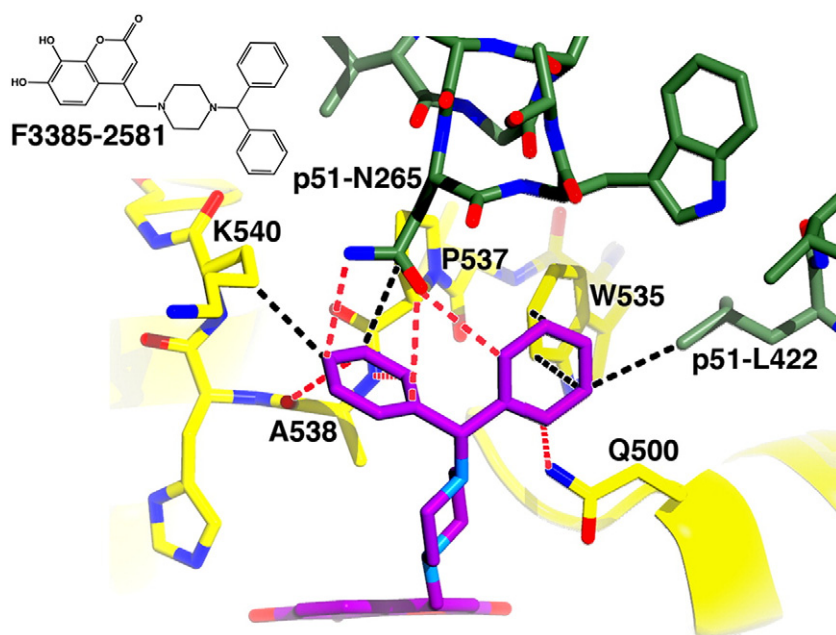


Fig. 5. Docking result for F3385-2581. The docking experiment resulted in one pose. Predicted electrostatic interactions (defined as hydrogen bonds, ionic–ionic, ionic–dipole, and dipole–dipole) are depicted by red dashes, and hydrophobic interactions are depicted by black dashes. Two additional hydrophobic contacts between residue Pro537 and the analog are not shown. An inset of the chemical structure is shown on the upper left side of the figure. Predicted protein–analog contacts were dominated by electrostatic interactions. An induced-fit Schrödinger Glide score of –10.25 was computed for this docking result.

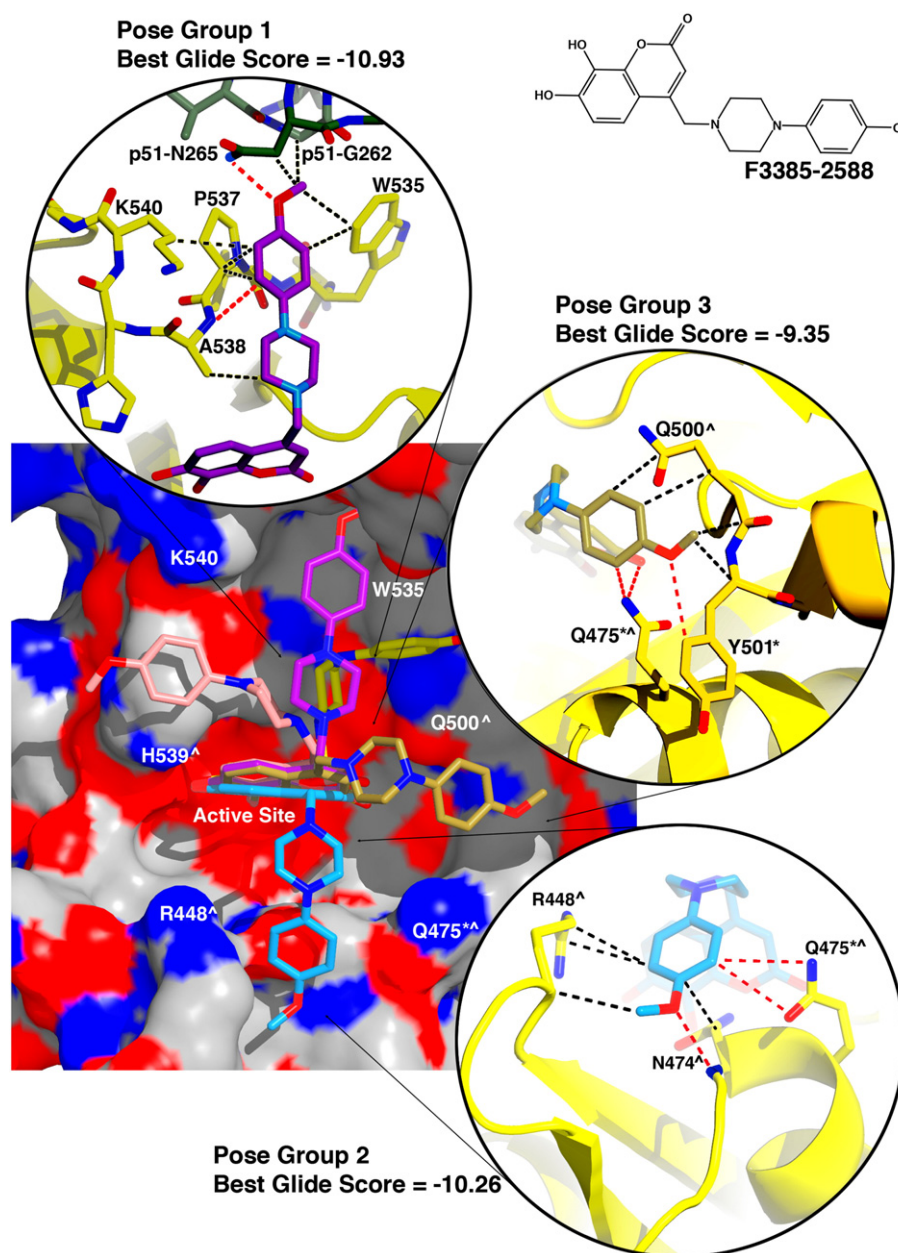


Fig. 6. Docking results for F3385-2588. An electrostatic potential surface diagram (calculated in PyMOL) is shown of RT with analog F3385-2588 docked to the RNase H active site. An inset of the chemical structure is shown on the upper right side of the figure. The induced-fit docking experiments resulted in multiple poses that could be categorized into several pose groups based on contacts formed with the protein. The most energetically favorable pose obtained for each of these groups is shown. Moving clockwise about the potential surface diagram, these pose groups interacted primarily with His539 and Ala538 (pink pose), Trp535 and Pro537 (violet “Pose Group 1”), Gln500 and Trp535 (yellow pose), Gln475 and Tyr501 (gold “Pose Group 3”), or Arg448 and Asn474 (cyan, “Pose Group 2”). For the top three docking results (Pose Groups 1–3), the Schrödinger Glide score is given (more negative = more energetically favorable), and insets are shown giving representative protein–inhibitor interactions predicted by the docking experiment (interactions color scheme as in Fig. 5). Residues of the RNase H primer grip are indicated by an asterisk (*), and residues that interact with the scissile phosphate of the substrate’s RNA strand (or with adjacent nucleotides) are indicated by a caret (^) [36].

interact with the DNA primer strand of an RNA:DNA substrate and may play a role in catalysis and RNA cleavage specificity [36]. Most of these predicted conformations featured both main-chain and side-

chain contacts with the inhibitor, including both hydrophobic and electrostatic interactions. The electrostatic contacts had a larger energetic component than the hydrophobic contacts in pose groups 2 and 3.

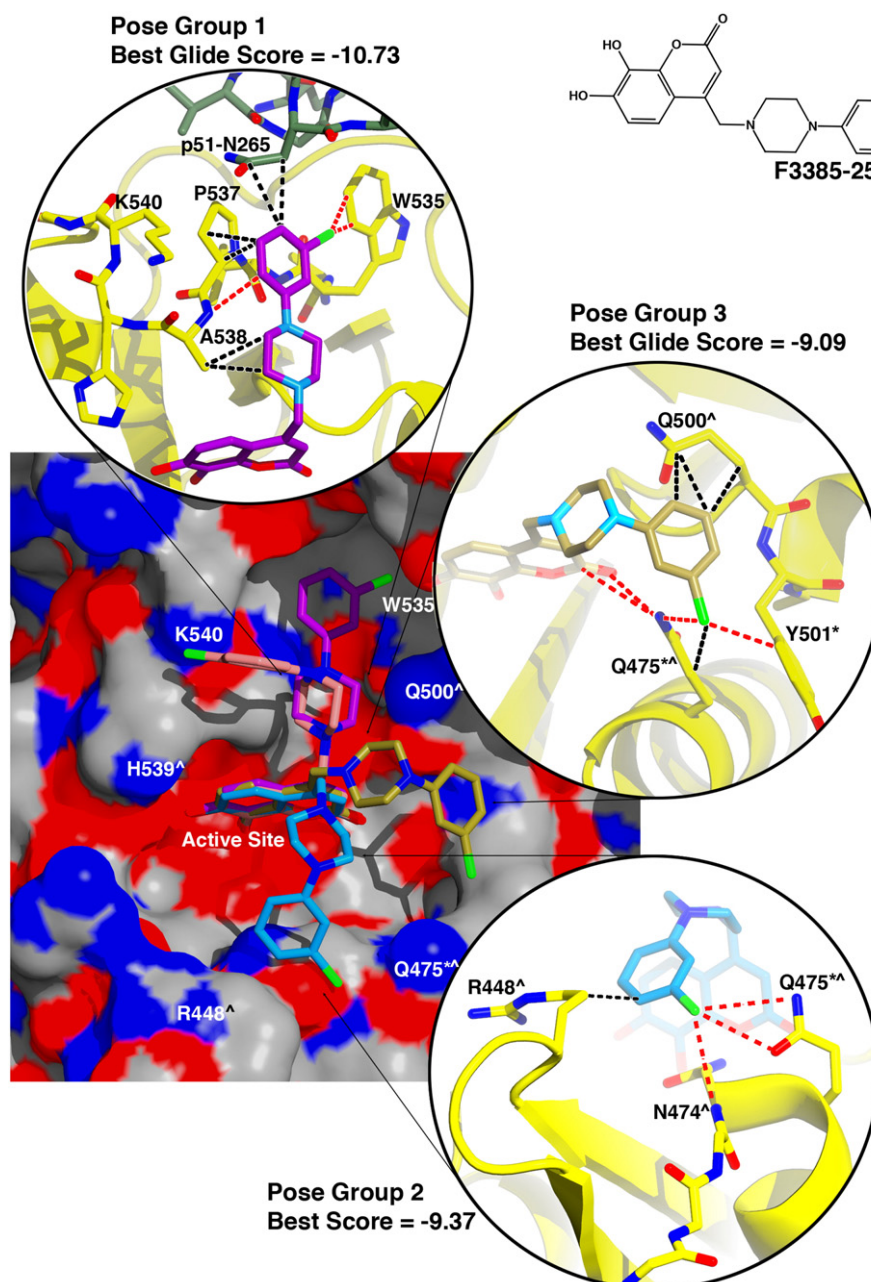


Fig. 7. Docking results for F3385-2590. An electrostatic potential surface diagram (calculated in PyMOL) is shown of RT with analog F3385-2590 docked to the RNase H active site. An inset of the chemical structure is shown on the upper right side of the figure. The resulting poses are similar to those obtained for F3385-2588 and are grouped as described in Fig. 6. The Schrödinger Glide scores are given for the top three scoring pose groups, and insets are shown giving representative protein-inhibitor interactions predicted by the docking experiment (interactions color scheme as in Fig. 5). Residues of the RNase H primer grip are indicated by an asterisk (*), and residues that interact with the scissile phosphate of the substrate's RNA strand (or with adjacent nucleotides) are indicated by a caret (^) [36].

Discussion and Conclusions

The RNase H active site is a shallow, solvent-exposed binding site that presents few binding opportunities for a ligand other than hydrophilic interactions. As a result, the site scores low as a

“druggable” binding site [17,35] using the Schrödinger Suite program SiteMap [37,38], which evaluates a binding pocket based on such factors as site enclosure and potential for hydrophobic and electrostatic interactions. In developing a highly effective RNase H active-site inhibitor, one strategy is to exploit

nearby regions of the RNase H domain to form favorable interactions or at least to optimize interactions with conserved active-site residues. Crystal structures have recently been reported for RNHIs with submicromolar inhibitory activity (a pyrimidinol carboxylic acid and an *N*-hydroxy-quinazolinedione) that both coordinate two Mn^{2+} cations at the active site and simultaneously form π – π interactions with the imidazole side chain of active-site residue His539 [17]. In addition, it is possible that two manicol derivatives with submicromolar inhibitory activity that coordinate Mn^{2+} cations at the RNase H active site also form favorable interactions with His539 [16].

We were interested in understanding in greater detail the structural basis for the difference between the inhibitory activity of F3284-8495 and other more active HIV RNHIs. We compared F3284-8495 to pyrimidinol carboxylic acid compound 1 (“3QIN #1”) [17], pyrimidinol carboxylic acid compound 2 (“3QIP #2”) [17], *N*-hydroxy-quinazolinedione (“3QIO #3”) [17], MK1 [15], MK2 [15], β -thujaplicinol [14,39], and manicol [16] (Table 4). Structures for all of these compounds exhibited very similar cation coordination geometry, although the inhibitory activities differed significantly. In particular, the cation coordination geometry and contact distances observed in the RNase H/F3284-8495 structure are practically identical (within 0.2 Å, except for one of the Asp498 carboxyl oxygens) to the geometry and distances observed in 3QIO #3 [17] and MK2 [15]. In spite of this similarity, the F3284-8495 inhibition of the RT RNase H activity is 20- to 40-fold weaker than the latter two compounds. The distance between cation A and cation B ranges from 3.5 Å (manicol) to 3.8 Å (3QIP #2, 3QIO #3) for all compounds examined here (including F3284-8495), with no linear relationship between this distance and inhibitory activity. In summary, it does not appear that any features of cation geometry and contact distances can be correlated consistently with differences in activities for the various inhibitors analyzed here.

On the other hand, a distinguishing feature of most of the more active inhibitors is the ability to form significantly more contacts with conserved residue His539 or other nearby amino acid residues than F3284-8495. F3284-8495 forms only eight contacts (<4.0 Å) with His539. By contrast, 3QIO #3 forms 22 interactions with His539 alone, and manicol forms 20 His539 contacts. MK1 has 11 contacts with His539. In addition, MK1, MK2, and 3QIP #3 form other amino acid contacts (such as Glu444, Ser499, Ala538, and Val552) not seen with the RNase H/F3284-8495 structure, including main-chain contacts.

Both the RNase H/F3284-8495 (Fig. 3) and the RT/ β -thujaplicinol [14] structures indicate a similar number of contacts with His539 and a similar number of protein–ligand contacts overall. However, of the two compounds only β -thujaplicinol inhibits an active RNase H domain and exhibits greater than 20-fold greater activity than F3284-8495 against the RNase H of full-length RT. One possible explanation for this difference could be that β -thujaplicinol may form a tropylium ion (in which it would carry a partial positive charge on its tropolone ring and a corresponding partial negative charge shared by its carbonyl and hydroxyl oxygen atoms), leading to a more productive interaction with His539 and tighter (more energetically favorable) binding to the RNase H active site than F3284-8495 [14]. In addition, it has previously been suggested that β -thujaplicinol might form favorable interactions with the nucleic acid substrate that further stabilize inhibitor binding [14]. In similar fashion, MK2 also appears capable of extensive interactions with the RNA strand of a nucleic acid substrate, based on superposition with an RT/RNA:DNA structure [36], but F3284-8495 does not appear capable of forming as many favorable interactions with substrate. Structures containing RT in complex with both the RNHI and nucleic acid substrate would be required to confirm this assessment. However, full-length RT binds nucleic acid more tightly than an RNase H domain fragment, and nucleic acid bound to RT could trap F3284-8495 at the RNase H binding site, so that the RNHI becomes active against the RNase H activity of full-length RT. In summary so far, good ligand efficiency at the RNase H active site may enhance inhibitory activity, including contacts with conserved active-site residues such as His539 and favorable interactions with the nucleic acid substrate that the ligand dislodges from the active site, whereas the exact geometry of divalent cation coordination does not appear to be as critical a factor to inhibitory potency. The advantage of F3284-8495 is that it is readily amenable to chemical modification and can be the basis for synthesizing compounds that interact more productively with the RNase H domain.

The computational analysis presented here suggests an alternative strategy. Although the most active F3284-8495 analogs have a derivative

Table 4. Comparison of F3284-8495 and some other RNHIs

Compound	PDB code	Resolution limit (Å)	IC ₅₀ , RT RNase H (μM)	Number of ligand–His539 contacts (<4.0 Å)
F3284-8495	4JE2	1.65	4.8	8
3QIN #1	3QIN	1.70	1.18	12
3QIP #2	3QIP	2.10	0.80	5
Manicol	3QLH	2.70	0.60	20
3QIO #3	3QIO	1.40	0.23	22
β -Thujaplicinol	3K2P	2.00	0.21	7
MK2	3LP1	2.20	0.12	8
MK1	3LP0	2.80	0.11	11

substructure long enough to reach key regions of the RNase H domain (such as the RNase H primer grip), the docking results favor a different possibility; namely, certain poses of these compounds assume binding modes that form contacts with residues of *both* the p66 and p51 subunits of RT along the cleft between the RNase H domain and the p51 subunit. This alternative is attractive because it presents a way to develop inhibitors that are selective for the RNase H domain of HIV-1 RT instead of interacting with human RNase H. For example, the scaffold of analog F3385-2588 suggests that building onto the methoxyphenyl substituent might enable exploitation of features on the p51 subunit, unique to HIV-1 RT.

Caution is warranted in the interpretation of these docking results. It is noteworthy that the highest-scoring docking results for F3284-8495 (Table 3) were not the best predictors of the observed crystal structure. Structures having slightly lower scores provided better agreement with the crystal structure and favored more plausible protonation states. This discrepancy between the crystal structure and the docking analysis may be due in part to the fact that Glide does not take into consideration either molecular strain or the energetics of water hydrogen-bonding networks before and after binding of the ligand. A newer version of Glide, which was not yet available during this work, attempts to address this shortcoming in part by incorporating a module called Watermap [40]. Thus, secondary docking results may provide a better representation of ligand interactions and should therefore be considered in addition to the highest-scoring conformations. As an example, pose groups 2 and 3 for F3385-2588 (Fig. 6) and F3385-2590 (Fig. 7) suggest that the inhibitors could interact with residues of the RNase H primer grip region that are vital for positioning the RNA:DNA substrate at the RNase H active site. All three analogs in Table 2 showed greater inhibition against the activity of the p15-EC RNase H than against the full-length RT RNase H, suggesting that the analog substructures do not interact as productively with full-length RT. This result suggests that all three analogs bind in a fashion that bring them in contact with residues outside of the RNase H domain, when binding to full-length RT, and indicates that these interactions would require considerable optimization. For the docking experiments with both F3385-2588 and F3385-2590, only pose 1 predicts contacts with residues outside of the RNase H domain (Figs. 6 and 7). It is unclear from the current analysis why interactions outside the RNase H domain would decrease inhibitory activity relative to p15-EC RNase H, but it is possible that conformational changes may occur across the cleft between the RNase H domain and the p51 subunit. Protein mutagenesis studies may clarify whether these ligand poses contribute to the observed inhibitory activities.

The piperazine rings of most analogs analyzed here give the inhibitor the ability to add some modest interactions with the protein, which could include hydrophobic interactions with Ala538. Functional groups attached to the distal nitrogen of the piperazine ring are capable of interacting with other RT residues, with the result that inhibitory activity improves compared to F3284-8495. For example, the docking results indicate that the chlorine atom on the terminal phenyl ring of F3385-2590 could form important electrostatic interactions with Trp535 or alternatively with Asn474 and Gln475 (Fig. 7). Based on pose 1, the chlorine on F3385-2590 leads to considerably more productive interactions with Trp535 than the terminal methoxyl group on F3385-2588. In the crystal structure, the side chain of Trp535 forms hydrophobic stacking interactions with the side chain of Pro537. The docking results suggest that compound F3385-2588 or F3385-2590 could replace Trp535 in contacts with Pro537, and Trp535 would become available for interactions with appropriately situated substituents on the terminal phenyl ring of the compound. Only in F3385-2590 is a halogen substituent present to take advantage of this opportunity. It may be possible to build a more bulky substituent in place of the chlorine atom to optimize hydrophobic interactions with Trp535 and spatially adjacent residues Leu422 and Trp426. Alternatively, it is possible that a derivative substructure would have additional interaction opportunities if it were linked to the F3284-8495 core by a two-methylene linker instead of the single methylene present in the analogs tested here. In that case, it might be possible to develop a branched substructure that could interact simultaneously with His539 and more distant residues, such as Trp535 and the p51 subunit of RT. F3284-8495 showed substantially increased inhibitory potency when assayed at pH 8.0 compared to pH 7.4. Our docking analysis is consistent with these biochemical data. The coumarin ring hydroxyls have pK_a values of about 8.9. The best agreement between a docked structure and the crystal structure of the RNase H/F3284-8495 complex occurred when the *ortho* hydroxyl of F3284-8495 was deprotonated.

Conclusions

F3284-8495 is a low micromolar specific inhibitor of the RNase H activity of HIV-1 RT. We used X-ray crystallography to determine the structure of this compound bound to the active site of an RNase H domain derived from HIV-1 RT. This structure was used to predict analogs with potentially improved binding; these analogs were obtained and many showed significantly improved inhibitory potency. This inhibition was more potent at pH values greater than physiological pH 7.4. Docking analyses suggested that this is due to the need for deprotonation of the coumarin ring *ortho* hydroxyl to provide an optimal

binding mode. Additional docking studies with analogs of F3284-8495 provided intriguing possibilities for ligand optimization involving interactions with Trp535 and residues in the p51 subunit of RT. This investigation provided proof of concept that synthesis based on the F3284-8495 scaffold could be used for development of new and possibly more potent RNHIs.

Materials and Methods

Materials

Compound F3284-8495 and analogs were purchased from Life Chemicals (Burlington, ON, Canada). All compounds were greater than 95% purity according to the supplier. Wild-type p66/p51 heterodimeric HIV-1 RT was expressed from plasmid p6HRT (a gift from Dr. S. Le Grice, National Cancer Institute Frederick, Frederick, MD) and purified essentially as previously described [41]. Plasmid pCSR231 encoding a codon-optimized chimeric HIV-1 RNase H domain fragment protein containing an α -helical substrate-binding loop derived from *E. coli* RNase HI [31–33] was a generous gift from Dr. Daria Hazuda (Merck, West Point, PA). This protein, termed p15-EC, was overexpressed and purified as previously described [34]. RT RDDP activity was measured as described previously [42]. RNase H activity of the RT heterodimer and the p15-EC RNase H domain fragment was determined using a rapid fluorescence assay [43].

Expression and purification of HIV-1 RT RNase H domain for structural studies

A plasmid encoding the HIV-1 RT RNase H domain (427–560) bearing an N-terminal 6 \times His tag (a kind gift from Karen Maegley, Pfizer) was transformed into the *E. coli* BL21 (DE3) pLysS bacterial strain and grown at 37 °C in 1 L Luria Broth with constant shaking at 280 rpm. When cells reached an OD₆₀₀ of 0.7–0.8, they were induced by addition of 1 mM IPTG and then left to grow for 4 h before they were harvested by centrifugation and stored at –20 °C.

Cells were resuspended in a buffer consisting of 20 mM Tris (pH 7.9), 300 mM NaCl, 20 mM imidazole, and 1 mM phenylmethylsulfonyl fluoride. Cells were lysed by sonication and the resulting lysate was centrifuged at 18,000 rpm (38,360g) for 30 min. The supernatant was recovered, filtered through a 0.45- μ m membrane, and then applied to a His-trap nickel column (GE Healthcare). The column was washed with at least 50 column volumes of lysis buffer and then eluted with 20 mM Tris (pH 7.9), 300 mM NaCl, and 250 mM imidazole. The eluate was concentrated to 1 mL and incubated with a 1:10 ratio of His-tagged tobacco etch virus protease overnight at 4 °C. The mixture was then injected back onto a His-trap column to remove the cleaved His tag and the tobacco etch virus protease. The flow-through was collected, concentrated to a volume of 1 mL, and injected onto a Superdex S200 size-exclusion column pre-equilibrated with 10 mM Tris (pH 8.0) and 75 mM NaCl. Fractions containing pure protein as

assessed by SDS-PAGE gel were pooled, concentrated to 20 mg/mL, and flash frozen at –80 °C.

Crystallization and data collection

The RNase H domain was crystallized at 20 °C (293 K) by vapor diffusion in hanging drops containing 2.0 mL each of protein solution (see above) and precipitant solution [100 mM Bicine (pH 8.2), 10 mM manganese sulfate, 1 mM sodium azide, and 9% (w/v) polyethylene glycol (PEG) 3350]. The drops were equilibrated over a reservoir containing 420 μ L of the precipitant solution to which 288 μ L of 50% (w/v) PEG 3350 was added. The chosen crystal was transferred stepwise to each of three soaking solutions that had in common 100 mM Bicine (pH 8.2), 10 mM manganese sulfate, 1 mM sodium azide, and 26% PEG 3350. The first soaking solution also contained 1% (v/v) glycerol and 5 mM F3284-8495, and the soak time was 3.5 h. The second and third soak solutions each contained 2.5 mM F3284-8495, as well as 13% and 27% glycerol, respectively. The soak time for the last two solutions was 15–20 s each. Finally, the crystal was flash-cooled and stored in liquid nitrogen. X-ray data were collected at 100 K and a wavelength of 1.1 Å at the National Synchrotron Light Source at Brookhaven National Laboratories, Beamline X25. The data were processed using DENZO/SCALEPACK [44,45].

Structure determination and refinement

Phases for the HIV-1 RNase H/F3284-8495 X-ray data were determined by molecular replacement with the CCP4 program PHASER [46,47], using as an initial search model an RNase H domain model derived from coordinates of RT in complex with β -thujaplicinol (PDB accession number: 3IG1) [14]. Stepwise structure refinement and model building were conducted using CNS 1.1 [48] with a bulk solvent correction and the Coot graphics package (version 0.6) [49]. The inhibitor coordinates were constructed and energy minimized using the Maestro™ graphics and Impact™ applications of the Schrödinger Software suite (Schrödinger, LLC) and were subsequently built into electron density maps using Coot, with ligand restraints generated by Sketcher in CCP4 [47]. Water molecules were built into the structure both manually and using the “Find Waters” tool of Coot. In later stages of refinement, both Phenix [50–52] and Schrödinger PrimeX [53] were utilized to overcome local energy minima and improve the geometry and placement of the inhibitor and Mn²⁺ atoms. Finally, anisotropic *B*-factor refinement and TLS refinement were carried out in Phenix.

Computational chemistry analysis

Selected compounds were constructed from the RNase H/F3284-8495 crystal structure coordinates of one of the asymmetric unit molecules and energy minimized using the Maestro™ graphics and Impact™ applications of the Schrödinger Software suite (Schrödinger, LLC). The compounds were subjected to steepest descent and then conjugate gradient energy minimization. The protonation states of each compound was analyzed in the Schrödinger Epik™ application over a pH range of 5.5–9.5, and each of the protonation states was prepared for docking using

Schrödinger LigPrep™. To prepare the protein receptor, we took RT subunit p51 residues 238–428 from the coordinates of a 1.8-Å-resolution RT structure (PDB code: 2ZD1) [54] and merged them with the current RNase H/F3284-8495 coordinates, using p66 residues 505–540 as the basis of superposition. The p51/p66 interface was energy minimized using the Schrödinger Prime™ module. Water molecules were removed, except for the two water molecules that coordinate Mn²⁺ cation A (Fig. 3). The receptor was merged with each compound to prepare a grid for docking.

To explore the conformational space of selected analogs of compound F3284-8495, it was assumed that the coumarin ring system of the analog interacts with the protein and Mn²⁺ cations exactly as observed in the crystal structure. The coumarin core (see Table 3) of each compound was aligned with that of the RNase H/F3284-8495 structure. Before preparing each grid, hydrogens were added and energy minimized with the Schrödinger “Protein Preparation Wizard Workflow” and Prime™. Docking was conducted using the Schrödinger Glide™ module, with imposition of coumarin core and metal coordination constraints to promote agreement with the crystal structure at the RNase H active site. Docking results with the most negative Glide scores and good core alignment with the crystal structure were subjected to induced-fit energy minimization using Prime. New grids were generated for the receptor, and the compounds were re-docked in Glide. Structure figures were generated using PyMOL [55].

Accession numbers

Coordinates and structure factors have been deposited in the Protein Data Bank with accession number 4QAG.

Supplementary data to this article can be found online at <http://dx.doi.org/10.1016/j.jmb.2014.05.006>.

Acknowledgements

This study was supported in part by grants from the National Institutes of Health (AI073975 to M.A.P.; R37AI27690 to E.A.) and an unrestricted grant (to M.A.P.) from Johnson & Johnson. We are grateful to Ronald M. Levy and members of his laboratory for providing auxiliary computer resources and advice. We wish to thank Karen A. Maegley at Pfizer, Inc. for generously providing us with an expression clone for an isolated RNase H domain for crystallographic studies and Dr. Daria Hazuda at Merck, Inc. for kindly providing us with an expression clone for the p15-EC RNase H domain for biochemical studies. Crystallographic data were collected at the National Synchrotron Light Source, Brookhaven National Laboratory. Use of the National Synchrotron Light Source, Brookhaven National Laboratory, was supported by the U.S. Department of Energy, Office of Science, Office of Basic Energy Sciences, under Contract No. DE-AC02-98CH10886.

Received 11 March 2014;

Received in revised form 8 May 2014;

Accepted 12 May 2014

Available online 17 May 2014

Keywords:

RNase H inhibitors;
dihydroxybenzopyrone derivatives;
HIV ribonuclease H;
protein–inhibitor complex;
structure-based drug design

Present address: D. M. Himmel, Department of Biochemistry,
Albert Einstein College of Medicine of Yeshiva University,
Bronx, NY 10461-1900, USA.

Present address: N. S. Myshakina, Department of Science,
Chatham University, Pittsburgh, PA 15232, USA.

Abbreviations used:

RNase H, ribonuclease H; HIV, human immunodeficiency virus; RT, reverse transcriptase; IPTG, isopropyl β-D-1-thiogalactopyranoside; PEG, polyethylene glycol; RDDP, RNA-dependent DNA polymerase; RNHI, RNase H inhibitor.

References

- [1] De Clercq E. Antiretroviral drugs. *Curr Opin Pharmacol* 2010;10: 507–15.
- [2] Singh K, Marchand B, Kirby KA, Michailidis E, Sarafianos SG. Structural aspects of drug resistance and inhibition of HIV-1 reverse transcriptase. *Viruses* 2010;2:606–38.
- [3] Jacobo-Molina A, Ding J, Nanni RG, Clark AD, Ju X, Tantillo C, et al. Crystal structure of human immunodeficiency virus type 1 reverse transcriptase complexed with double-stranded DNA at 3.0 Å resolution shows bent DNA. *Proc Natl Acad Sci USA* 1993;90:6320–4.
- [4] Tisdale M, Schulze T, Larder BA, Moelling K. Mutations within the RNase H domain of HIV-1 RT abolish virus infectivity. *J Gen Virol* 1991;72:59–66.
- [5] Schatz O, Cromme F, Naas T, Lindermann D, Gruninger-Leitch F, Mous J, et al. Inactivation of the RNase H domain of HIV-1 reverse transcriptase blocks viral infectivity. In: Papas T, editor. *Oncogenesis and AIDS*. Houston, TX: Portfolio Publishing Company; 1990. p. 55–68.
- [6] Ghosn J, Chaix ML, Delaugerre C. HIV-1 resistance to first- and second-generation non-nucleoside reverse transcriptase inhibitors. *AIDS Rev* 2009;11:165–73.
- [7] Adams J, Patel N, Mankaryous N, Tadros M, Miller CD. Nonnucleoside reverse transcriptase inhibitor resistance and the role of the second-generation agents. *Ann Pharmacother* 2010;44:157–65.
- [8] Gong J, Wang XQ, Tong X, Shen XH, Yang RG. Emerging trends of drug-resistant HIV-1 among drug-treated patients in former blood donors in Hubei, China: a three-year surveillance from 2004 to 2006. *Virol Sin* 2011;26:386–92.
- [9] Menéndez-Arias L, Betancor G, Matamoros T. HIV-1 reverse transcriptase connection subdomain mutations involved in resistance to approved non-nucleoside inhibitors. *Antiviral Res* 2011;92:139–49.

- [10] Singh K, Marchand B, Rai DK, Sharma B, Michailidis E, Ryan EM, et al. Biochemical mechanism of HIV-1 resistance to Rilpivirine. *J Biol Chem* 2012;287:38110–23.
- [11] Himmel DM, Sarafianos SG, Dharmasena S, Hossain MM, McCoy-Simandle K, Ilina T, et al. HIV-1 reverse transcriptase structure with RNase H inhibitor dihydroxy benzoyl naphthyl hydrazone bound at a novel site. *ACS Chem Biol* 2006;1: 702–12.
- [12] Klumpp K, Mirzadegan T. Recent progress in the design of small molecule inhibitors of HIV RNase H. *Curr Pharm Des* 2006;12:1909–22.
- [13] Kirschberg TA, Balakrishnan M, Squires NH, Barnes T, Brendza KM, Chen X, et al. RNase H active site inhibitors of human immunodeficiency virus type 1 reverse transcriptase: design, biochemical activity, and structural information. *J Med Chem* 2009;52:5781–4.
- [14] Himmel DM, Maegley KA, Pauly TA, Bauman JD, Das K, Dharia C, et al. Structure of HIV-1 reverse transcriptase with the inhibitor beta-thujaplicinol bound at the RNase H active site. *Structure* 2009;17:1625–35.
- [15] Su HP, Yan Y, Prasad GS, Smith RF, Daniels CL, Abeywickrema PD, et al. Structural basis for the inhibition of RNase H activity of HIV-1 reverse transcriptase by RNase H active site-directed inhibitors. *J Virol* 2010;84:7625–33.
- [16] Chung S, Himmel DM, Jiang JK, Wojtak K, Bauman JD, Rausch JW, et al. Synthesis, activity, and structural analysis of novel alpha-hydroxytropolone inhibitors of human immunodeficiency virus reverse transcriptase-associated ribonuclease H. *J Med Chem* 2011;54:4462–73.
- [17] Lansdon EB, Liu Q, Leavitt SA, Balakrishnan M, Perry JK, Lancaster-Moyer C, et al. Structural and binding analysis of pyrimidinol carboxylic acid and N-hydroxy quinazolinone HIV-1 RNase H inhibitors. *Antimicrob Agents Chemother* 2011;55:2905–15.
- [18] Kleywegt GJ, Brünger AT. Checking your imagination: applications of the free R value. *Structure* 1996;4:897–904.
- [19] Kleywegt GJ, Bergfors T, Senn H, LeMotte P, Gsell B, Shudo K, et al. Crystal structures of cellular retinoic acid binding proteins I and II in complex with all-trans-retinoic acid and a synthetic retinoid. *Structure* 1994;2:1241–58.
- [20] Luzzati V. Traitement statistique des erreurs dans la détermination des structures cristallines. *Acta Crystallogr* 1952;5:802–10.
- [21] Engh RA, Huber R. Accurate bond and angle parameters for X-ray protein structure refinement. *Acta Crystallogr Sect A Found Crystallogr* 1991;47:392–400.
- [22] Schatz O, Cromme FV, Gruninger-Leitch F, Le Grice SFJ. Point mutations in conserved amino acid residues within the C-terminal domain of HIV-1 reverse transcriptase specifically repress RNase H function. *FEBS Lett* 1989;257:311–4.
- [23] Davies JF, Hostomska Z, Hostomsky Z, Jordan SR, Matthews DA. Crystal structure of the ribonuclease H domain of HIV-1 reverse transcriptase. *Science* 1991;252:88–95.
- [24] Nowotny M, Gaidamakov SA, Crouch RJ, Yang W. Crystal structures of RNase H bound to an RNA/DNA hybrid: substrate specificity and metal-dependent catalysis. *Cell* 2005;121:1005–16.
- [25] Nowotny M, Gaidamakov SA, Ghirlando R, Cerritelli SM, Crouch RJ, Yang W. Structure of human RNase H1 complexed with an RNA/DNA hybrid: insight into HIV reverse transcription. *Mol Cell* 2007;28:264–76.
- [26] Yang W, Hendrickson WA, Crouch RJ, Satow Y. Structure of ribonuclease H phased at 2 Å resolution by MAD analysis of the selenomethionyl protein. *Science* 1990;249:1398–405.
- [27] Steitz TA, Steitz JA. A general two-metal-ion mechanism for catalytic RNA. *Proc Natl Acad Sci USA* 1993;90:6498–502.
- [28] Bauman JD, Das K, Ho WC, Baweja M, Himmel DM, Clark AD, et al. Crystal engineering of HIV-1 reverse transcriptase for structure-based drug design. *Nucleic Acids Res* 2008;36:5083–92.
- [29] Kuroda DG, Bauman JD, Challa JR, Patel D, Troxler T, Das K, et al. Snapshot of the equilibrium dynamics of a drug bound to HIV-1 reverse transcriptase. *Nat Chem* 2013;5:174–81.
- [30] Himmel DM, Das K, Clark AD, Hughes SH, Benjahad A, Oumouch S, et al. Crystal structures for HIV-1 reverse transcriptase in complexes with three pyridinone derivatives: a new class of non-nucleoside inhibitors effective against a broad range of drug-resistant strains. *J Med Chem* 2005;48:7582–91.
- [31] Keck JL, Marqusee S. Substitution of a highly basic helix/loop sequence into the RNase H domain of human immunodeficiency virus reverse transcriptase restores its Mn(2+)-dependent RNase H activity. *Proc Natl Acad Sci USA* 1995;92:2740–4.
- [32] Stahl SJ, Kaufman JD, Vikic-Topic S, Crouch RJ, Wingfield PT. Construction of an enzymatically active ribonuclease H domain of human immunodeficiency virus type 1 reverse transcriptase. *Protein Eng* 1994;7:1103–8.
- [33] Shaw-Reid CA, Munshi V, Graham P, Wolfe A, Witmer M, Danzeisen R, et al. Inhibition of HIV-1 ribonuclease H by a novel diketo acid, 4-[5-(benzoylamino)thien-2-yl]-2,4-dioxobutanoic acid. *J Biol Chem* 2003;278:2777–80.
- [34] Gong Q, Menon L, Ilina T, Miller LG, Ahn J, Parniak MA, et al. Interaction of HIV-1 reverse transcriptase ribonuclease H with an acylhydrazone inhibitor. *Chem Biol Drug Des* 2011;77: 39–47.
- [35] Felts AK, Labarge K, Bauman JD, Patel DV, Himmel DM, Arnold E, et al. Identification of alternative binding sites for inhibitors of HIV-1 ribonuclease H through comparative analysis of virtual enrichment studies. *J Chem Inf Model* 2011;51:1986–98.
- [36] Sarafianos SG, Das K, Tantillo C, Clark AD, Ding J, Whitcomb JM, et al. Crystal structure of HIV-1 reverse transcriptase in complex with a polypurine tract RNA:DNA. *EMBO J* 2001;20:1449–61.
- [37] Halgren T. New method for fast and accurate binding-site identification and analysis. *Chem Biol Drug Des* 2007;69: 146–8.
- [38] Halgren TA. Identifying and characterizing binding sites and assessing druggability. *J Chem Inf Model* 2009;49:377–89.
- [39] Budihas SR, Gorshkova I, Gaidamakov S, Wamiru A, Bona MK, Parniak MA, et al. Selective inhibition of HIV-1 reverse transcriptase-associated ribonuclease H activity by hydroxylated tropolones. *Nucleic Acids Res* 2005;33:1249–56.
- [40] Repasky MP, Murphy RB, Banks JL, Greenwood JR, Tubert-Brohman I, Bhat S, et al. Docking performance of the Glide program as evaluated on the Astex and DUD datasets: a complete set of Glide SP results and selected results for a new scoring function integrating Watermap and Glide. *J Comput Aided Mol Des* 2012;26:787–99.
- [41] Fletcher RS, Holleschak G, Nagy E, Arion D, Borkow G, Gu Z, et al. Single-step purification of recombinant wild-type and mutant HIV-1 reverse transcriptase. *Protein Expression Purif* 1996;7:27–32.
- [42] Borkow G, Fletcher RS, Barnard J, Arion D, Motakis D, Dmitrienko GI, et al. Inhibition of the ribonuclease H and DNA polymerase activities of HIV-1 reverse transcriptase by N-(4-tert-butylbenzoyl)-2-hydroxy-1-naphthaldehyde hydrazone. *Biochem* 1997;36:3179–85.

- [43] Parniak MA, Min KL, Budihas SR, Le Grice SF, Beutler JA. A fluorescence-based high-throughput screening assay for inhibitors of human immunodeficiency virus-1 reverse transcriptase-associated ribonuclease H activity. *Anal Biochem* 2003;322:33–9.
- [44] Otwinowski Z, Minor W, Borek D, Cymborowski M. DENZO and SCALEPACK. In: Arnold E, Himmel DM, Rossmann MG, editors. *International Tables for Crystallography Volume F: Crystallography of Biological Macromolecules*. 2nd edit. West Sussex, United Kingdom: John Wiley & Sons, Ltd; 2012. p. 282–95.
- [45] Otwinowski Z, Minor W. Processing of X-ray diffraction data collected in oscillation mode. *Methods Enzymol* 1997;276: 307–26.
- [46] Read RJ. Pushing the boundaries of molecular replacement with maximum likelihood. *Acta Crystallogr Sect D Biol Crystallogr* 2001;57:1373–82.
- [47] Winn MD, Ballard CC, Cowtan KD, Dodson EJ, Emsley P, Evans PR, et al. Overview of the CCP4 suite and current developments. *Acta Crystallogr Sect D Biol Crystallogr* 2011;67:235–42.
- [48] Brünger AT, Adams PD, Clore GM, DeLano WL, Gros P, Grosse-Kunstleve RW, et al. Crystallography and NMR system: a new software suite for macromolecular structure determination. *Acta Crystallogr Sect D Biol Crystallogr* 1998;54:905–21.
- [49] Emsley P, Lohkamp B, Scott WG, Cowtan K. Features and development of Coot. *Acta Crystallogr Sect D Biol Crystallogr* 2010;66:486–501.
- [50] Adams PD, Afonine PV, Bunkoczi G, Chen VB, Davis IW, Echols N, et al. PHENIX: a comprehensive Python-based system for macromolecular structure solution. *Acta Crystallogr Sect D Biol Crystallogr* 2010;66:213–21.
- [51] Moriarty NW, Grosse-Kunstleve RW, Adams PD. Electronic Ligand Builder and Optimization Workbench (eLBOW): a tool for ligand coordinate and restraint generation. *Acta Crystallogr Sect D Biol Crystallogr* 2009;65:1074–80.
- [52] Afonine PV, Grosse-Kunstleve RW, Echols N, Headd JJ, Moriarty NW, Mustyakimov M, et al. Towards automated crystallographic structure refinement with Phenix.Refine. *Acta Crystallogr Sect D Biol Crystallogr* 2012;68:352–67.
- [53] Bell JA, Cao Y, Gunn JR, Day T, Gallicchio E, Zhou Z, et al. PrimeX and the Schrödinger Computational Chemistry Suite of Programs. In: Arnold E, Himmel DM, Rossmann MG, editors. *International Tables for Crystallography Volume F: Crystallography of Biological Macromolecules*. 2nd edit. West Sussex, United Kingdom: John Wiley & Sons, Ltd; 2012. p. 534–8.
- [54] Das K, Bauman JD, Clark AD, Frenkel YV, Lewi PJ, Shatkin AJ, et al. High-resolution structures of HIV-1 reverse transcriptase/TMC278 complexes: strategic flexibility explains potency against resistance mutations. *Proc Natl Acad Sci USA* 2008;105:1466–71.
- [55] DeLano WL. The PyMOL Molecular Graphics System. DeLano Scientific; 2002.